IOP Conf. Series: Earth and Environmental Science **774** (2021) 012007 doi:10.1088/1755-1315/774/1/012007

Volute throat area and wall modelling influence on the numerical performances of a very low specific speed pump

Lilian Chabannes, David Štefan, Pavel Rudolf
Brno University of Technology, Kaplan Department of Fluid Engineering, Czech Republic
E-mail: 207556@vutbr.cz

Abstract. Low specific speed pumps find applications in a broad range of domains, but suffer from a low efficiency and a risk of head instability close to shut-off. The numerical computations on these pumps performed in the last years have shown discrepancies with experimental results. Recent studies suggest that the use of wall-functions underpredicts the losses of these pumps, especially at overload. The reason has been attributed to a detachment zone downstream the volute tongue, not well captured with the wall-function approach. This paper focuses on the influence of the volute casing on a pump with a specific speed of 8.9 on two issues. First, the influence of the wall modelling approach relatively to the low-Reynolds number method on the performance prediction is discussed. The results are, as expected, an underprediction of the losses when the wall-function approach is used. With a larger volute, the difference between the two wall modeling approaches is smaller. Secondly, the influence of the volute throat area enlargement on the pump performances is discussed. Both the head and efficiency are improved at the design point and at overload with an increased volute throat area. However the part-load head decreases and the head flattens. The study of the flow at part-load, in the region at the outlet of the impeller reveals that with a larger volute, larger flow exchanges are present, contributing to additional mixing losses and head loss.

1. Introduction

The design of low specific speed (LSS) pumps presents many challenges. A typical large impeller diameter causes considerable disk friction and volute losses, reducing the optimal efficiency. These pumps are also prone to partload head instability, where a positive head slope close to shut-off can be observed ($dH/dQ > 0$). The numerical computations of such pumps also proved to be a rough task. Large errors between experiments and computations have been reported [1] [2].

Juckelandt [3] studied the applicability of wall functions in a pump with a specific speed of $n_q = 12$. The results revealed that the wall function approach (WF) overestimated the head and the efficiency, especially at overload. With the use of a mesh resolving the boundary layer with the low-Reynolds number method (LR), the computations properly matched the experiments. Applying the WF approach to LSS pumps tends to predict the best efficiency point (BEP) at higher flow rate. The head is observed to be up to 50% higher at overload. The reason for great overload discrepancies is attributed to erroneous loss prediction downstream the volute tongue. A detachment zone with high turbulence kinetic energy (TKE) is not captured by the WF approach.

Content from this work may be used under the terms of the Creative Commons Attribution 3.0 licence. Any further distribution of this work must maintain attribution to the author(s) and the title of the work, journal citation and DOI.
Published under licence by IOP Publishing Ltd

Losses due to wall roughness are of importance at low specific speed, especially in the sidewall gaps and in the volute casing [4] [5]. Its effect has also been studied by Juckelandt [6] for the same pump of $n_q = 12$. The reported experiments with hydraulically smooth and rough (sand casted) walls had reduced performances with rough walls. At the design point, the head is decreased by 3% and the efficiency by 10%. The performance loss gets slightly larger with increasing flow rate, as an additional 1% decrease is observed at $Q/Q_d = 1.4$ for both the head and the efficiency.

The volute casing plays a more important role for low specific speed pumps. It mainly determines the position of the BEP and largely adds to losses. Worster [4] evaluated the volute losses as:

$$\frac{\Delta h_{L,vol}}{H} = f\frac{V^2}{2gH}\frac{S_{vol}}{A_{vs}} \tag{1}$$

From specific speed ranging from $n_q = 10$ to $n_q = 65$, typical values for the first ratio $\frac{V^2}{2gH}$ drops from 0.2 to 0.09 while the second ratio $\frac{S_{vol}}{A_{vs}}$ drops from 200 to 20. This second part is directly due to the volute having a large wetted surface S_{vol} to adapt to the large impeller diameter, with a small throat area A_{vs} due to the small flow rate. This also explains the large importance of friction at low specific speed.

Studies of the influence of the volute throat area have been performed several times in the past. Worster [4] and Khoeini [7] showed that an increase in volute area will reduce the shut-off head and increase the head at larger flow rate, subsequently flattening the head curve.

This paper has two motivation. One is to confirm the behaviour observed by Juckelandt [3], stating that the wall-function approach leads to strong discrepancies relatively to the low-Reynolds number method where the boundary layer is resolved. Only numerical results are available and the effects of roughness are neglected. The second objective is to investigate the influence of the volute throat area enlargement on a very low specific speed pump, and evaluate its influence on the main pump performance parameters.

2. Geometry and numerical methods

2.1. Pump model

The pump, on which computations are performed in this paper, has a specific speed $n_q = 8.9$. The different pump parameters can be seen in Table 1. The impeller and volute have been designed with an in-house code based on quasi-potential flow theory [8] [9].

The design of the 3 volute (V_1, V_2, V_3) is based on Anderson and Worster criteria, see Figure 2. The grey area represents the recommended ratio A_{vs}/A_{II} as a function of n_q for optimal efficiency. The area A_{II} is given by the impeller geometry:

$$A_{II} = \pi d_2 b_2 sin(\beta_{2B}) \tag{2}$$

Different ratios A_{vs}/A_{II} are obtained by changing the input flow rate for the specific speed. The new ratio based on the new calculated specific speed is read from figure 2, and a new volute throat area is obtained. The input flow rates are taken as Q_d, $2Q_d$ and $3Q_d$, respectively giving volute throat areas marked A_{vs_1}, A_{vs_2} and A_{vs_3}. The volute development is constructed based on the classic rule of constant angular momentum. The other volute parameters, such as the volute inlet width, tongue position and diameter, are calculated from Gülich recommendations [5], and kept constant for the three designs, so that only volute area development and the volute throat area are changed between the three designs. Figure 1 presents a cross-section of the different components of the pump, showing the sections of the 3 volutes.

Table 1. Pump parameters

Designation	Symbol	Value	Units
Rotor speed	N	1450	RPM
Design head	H_d	32	m
Design flow rate	Q_d	0.0069	$m^3.s^{-1}$
Specific speed	$n_q = N\frac{Q_d^{0.5}}{H_d^{0.75}}$	8.9	-
Impeller outlet diameter	d_2	320	mm
Impeller outlet width	b_2	6	mm
Impeller outlet blade angle	β_{2B}	25	deg
Volute throat Area 1	A_{vs_1}	496	mm^2
Volute throat Area 2	A_{vs_2}	670	mm^2
Volute throat Area 3	A_{vs_3}	806	mm^2

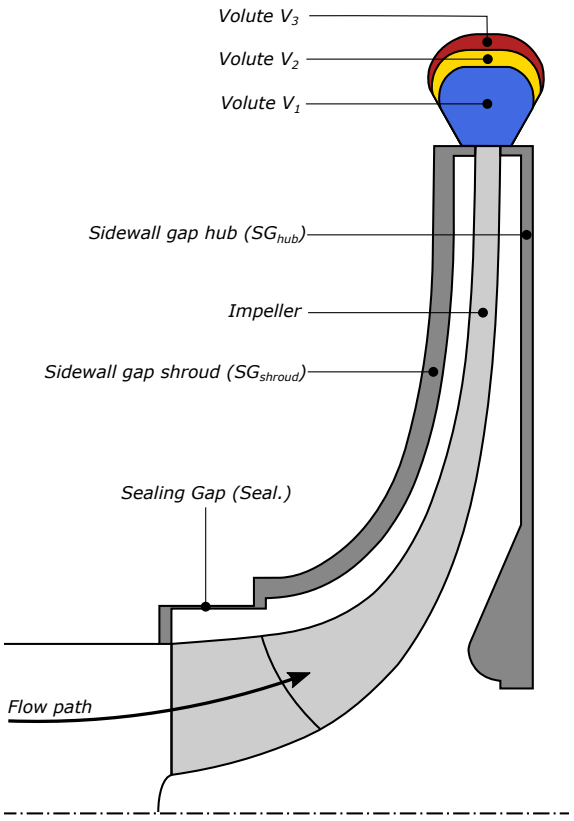

Figure 1. Section of fluid domains.

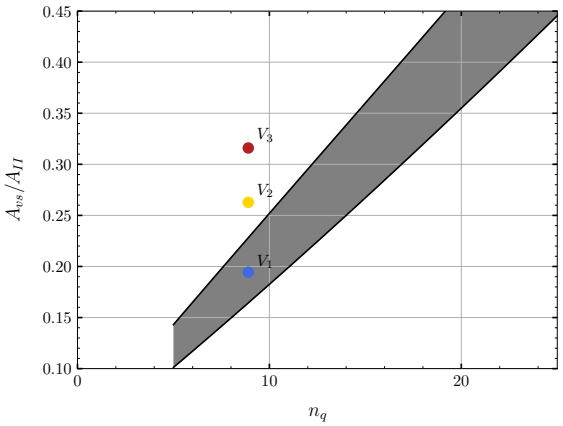

Figure 2. Volute throat area ratio vs. specific speed.

2.2. Mesh and CFD specification

The pump is modelled with a mesh adopting the Low-Reynolds number method (LR) to resolve the boundary layer, and a mesh modelling the boundary layer with the wall function approach (WF). For a given wall treatment method, only the volute geometry and mesh are changed. With 3 volute geometries (V_1, V_2, V_3) and 2 different wall treatment methods (WF, LR), a total of 6 cases are made, and noted $V_{1,WF}$, $V_{1,LR}$, $V_{2,WF}$, $V_{2,LR}$, $V_{3,WF}$, $V_{3,LR}$.

The meshes of the different fluid domains are created using the pre-processor ICEM-HEXA,

except for the impeller, where ANSYS-TurboGrid is used. A mesh sensitivity analysis is performed for the case $V_{1,LR}$. The wall requirement respects the condition $y^+ \leq 1$ almost at all surfaces, except at the trailing edge of the impeller blades, where flow separation is obvious. Figure 4 presents the results of y^+ for the chosen mesh where the sidewall gaps have been excluded for visualization clarity. During the mesh convergence analysis, the first cell height is kept constant not to affect the wall treatment, and the core mesh is uniformly changed in the domains. The torque τ, head H and hydraulic efficiency η are measured, and the results are shown in Figure 3. The final mesh has a total of 16.6 million hexahedral cells, and can be fully seen in Figure 5.

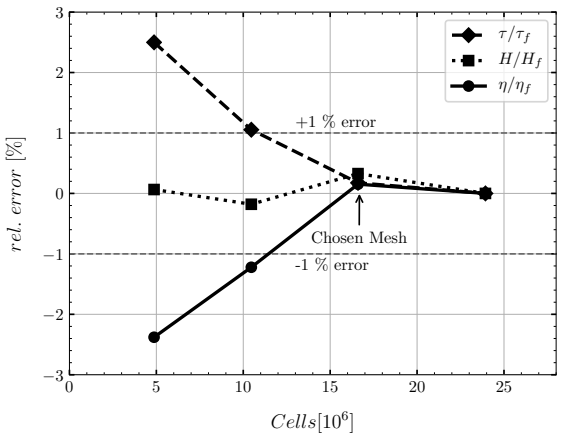

Figure 3. Mesh convergence analysis.

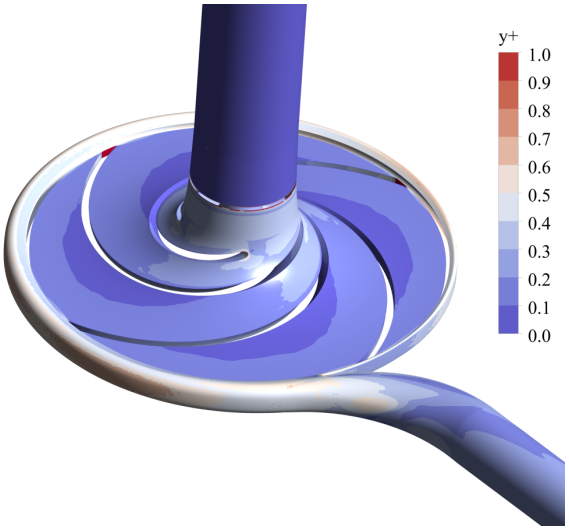

Figure 4. y^+ for $V_{1,LR}$ at $Q = Q_d$.

For meshes using the WF method, only the first cell height is changed, and is about 140 times bigger to achieve a y^+ between 30 and 300 everywhere. The case $V_{1,WF}$ has 4.2 millions cells, 4 times less than the case using the LR approach.

ANSYS-CFX is used to perform the computation. The turbulence model used is $k-\omega$ SST by Menter [10] with automatic wall-treatment. The curvature-correction option is set. Steady state simulations are used as initial conditions for transient simulations where the timestep is fixed to 1.5° of impeller rotation per timestep, or 1.72 10^{-4} s. The RMS residuals are set to 10^{-5}. The steady state behaviour of the pumps is of interest in this paper, thus all results and flow field have been time-averaged over the last 5 impeller rotations, after a cyclic behaviour is observed. 6 flow rates are computed for each case, from 10% to 160% of the design flowrate. The total number of unsteady computations is 36 (6 flow rates, 3 different volute, 2 wall treatment methods).

3. Wall functions vs. Low-Reynolds number approach for wall treatment

A comparison between the two wall treatment methods is performed. The difference of performance prediction for both methods is evaluated. For a quantity ϕ, the calculation is as follows:

$$\Delta_\phi = \frac{\phi_{WF} - \phi_{LR}}{\phi_{LR}} \cdot 100\% \tag{3}$$

The difference Δ_ϕ is evaluated for the head and the hydraulic efficiency over the whole operating range for the 3 different volutes. Figure 6 presents the results.

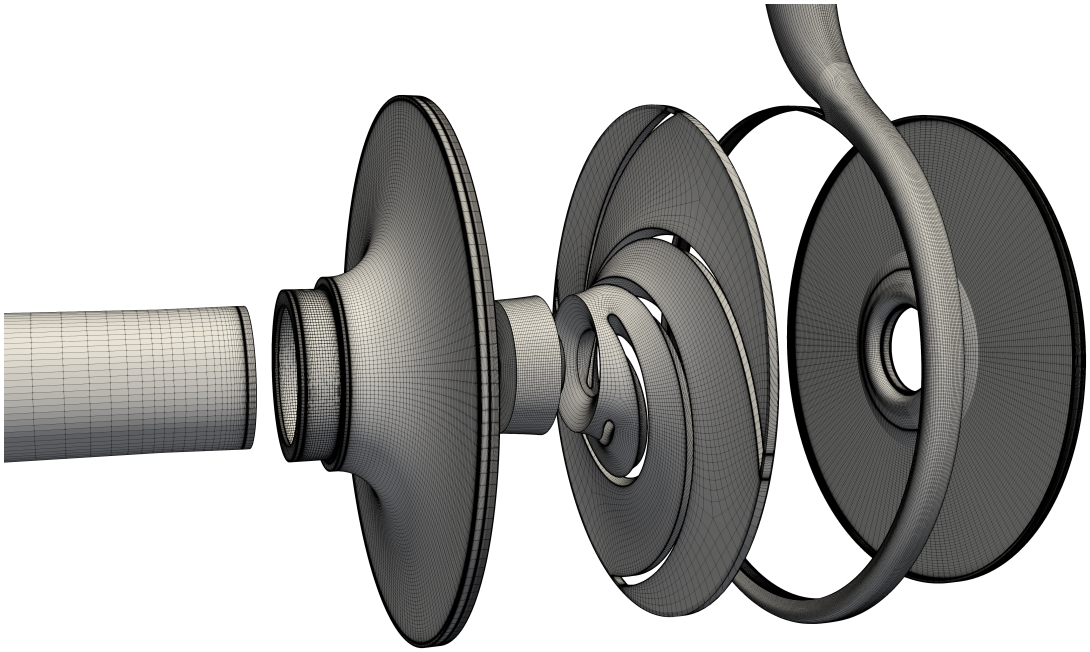

Figure 5. View of the grid for the case $V_{1,LR}$.

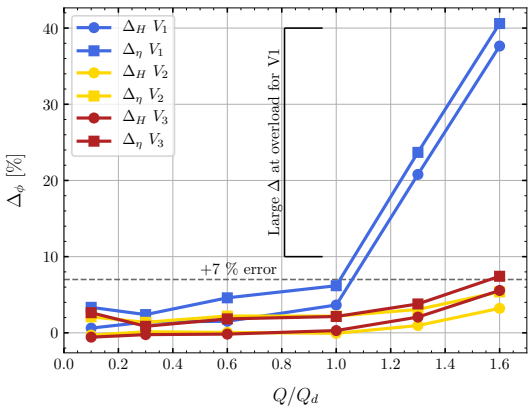

Figure 6. Difference Δ_ϕ for cases V_1, V_2 and V_3.

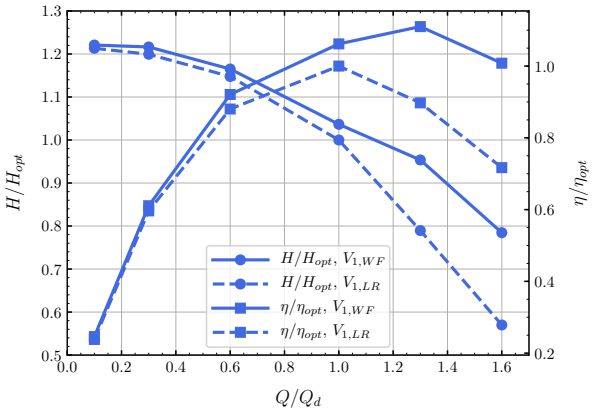

Figure 7. Head and efficiency of the cases $V_{1,WF}$ and $V_{1,LR}$

At partload, Δ_ϕ is reasonably low for all cases, especially for the hydraulic efficiency. At the design point, the error increases for V_1, while staying low for the other cases. At overload, Δ_ϕ dramatically rises to more than 20%. The difference increases with the flow rate for volutes V_2 and V_3 as well and the same behaviour is observed, but is comparatively low with an error of about 5% and 7% for V_2 and V_3 respectively at $Q/Q_d = 1.6$. The value of Δ_ϕ is always positive for the head and the efficiency, indicating that the WF approach over-predicts the performances comparing to the LR approach.

To understand the reason behind the large discrepancies at overload, the losses $P_{L,i}$ in each domain i are computed, as done in [3]. The losses in the inlet pipe are neglected.

$$P_{L,i} = \sum P_{\tau,i} + P_{in/out,i} \tag{4}$$

$P_\tau = \omega\tau$ is the power transferred to the fluid measured at rotating walls and $P_{in/out} = \int \frac{p_T}{\rho} d\dot{m}$ measures the power entering and leaving a domain. The losses are scaled by the total losses of the case $V_{1,LR}$, noted $P_{L_{TOT,V_{1,LR}}}$. The results are presented at overload, at $Q/Q_d = 1.6$ in Figure 8. For the three volutes, the losses are usually slightly higher in every domain for LR cases. However, the main differences between WF and LR is located in the volute. This confirms that the large Δ_ϕ observed in the head and hydraulic efficiency at overload is due to the prediction of volute losses. The same behaviour is observed for cases V_2 and V_3, with a lesser difference in loss predictions. The turbulent kinetic energy (TKE) is plotted in Figure 9 to identify the region with high losses. Clearly, high TKE is observed downstream the tongue, where detachment and mixing is known to happen at overload. For the three volutes, the TKE is larger for LR computation, especially for V_1.

The behaviour observed by Juckelandt [3] is also observed here. For the first case V_1, the BEP is clearly displaced to higher flow rates as seen in Figure 7. The same behaviour is present for other volute at a lower scale, and the performance prediction for both wall treatments is closer. The WF erroneous predictions seem to be linked to the flow physics. Enlarging the throat area reduces the velocity downstream the tongue and the zone of large TKE, where detachment also occurs. The prediction between WF and LR also decreases, but the pump performances are affected by different volutes.

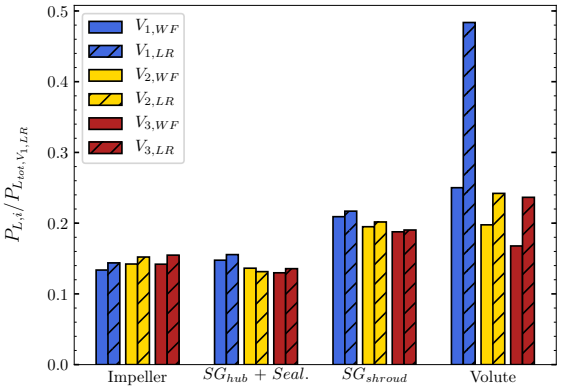

Figure 8. Relative losses per domain and per case as per equation 4 at $Q/Q_d = 1.6$.

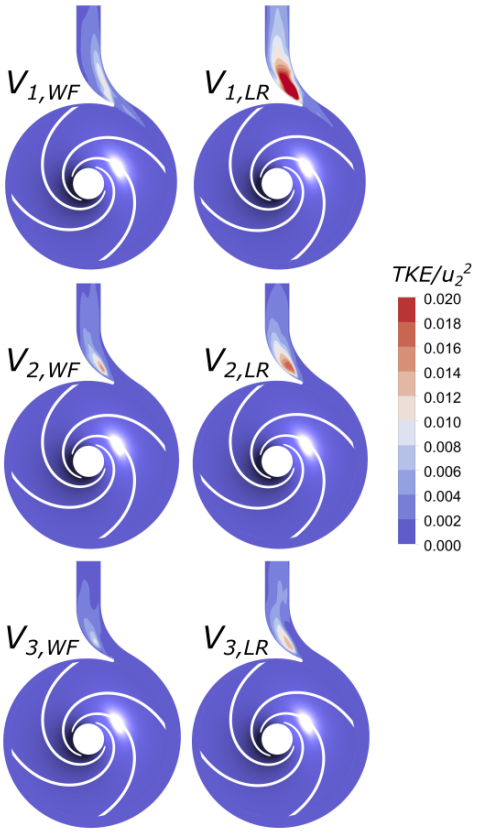

Figure 9. Scaled TKE for all cases at $Q/Q_d = 1.6$.

4. Volute throat area influence on the pump performance

In this section, only results obtained with the Low-Reynolds number approach are discussed.

The head and efficiency for the 3 cases are presented in figures 10 - 11. As the volute dimension increases, the head at partload diminishes, and the head at overload increases, leading to a flattening of the head curve. The efficiency is slightly lower at partload and the BEP is displaced to higher flow rates. Although the expected behaviour is verified, it is not linear between the three volutes, as $V_{2,LR}$ and $V_{3,LR}$ have similar predicted head and hydraulic efficiency with a large difference comparing to $V_{1,LR}$. The volute enlargement is beneficial at the design point and at overload, where both the head and the efficiency are improved. The physics for such performance improvement is discussed in the previous part. A larger volute, in particular a large volute throat area, reduces TKE downstream the tongue, as it can be seen by looking at the right side of figure 9.

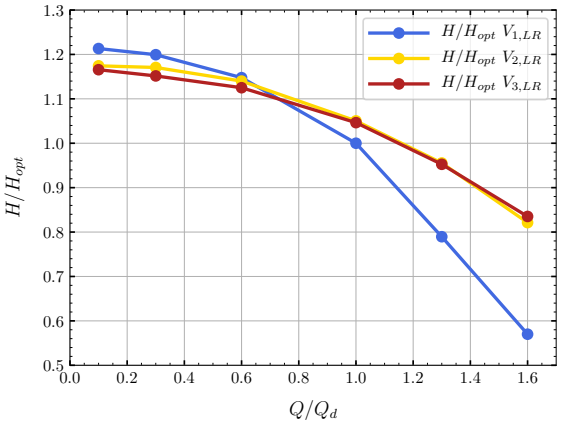

Figure 10. Head calculated by CFD for Low-Reynolds number meshes.

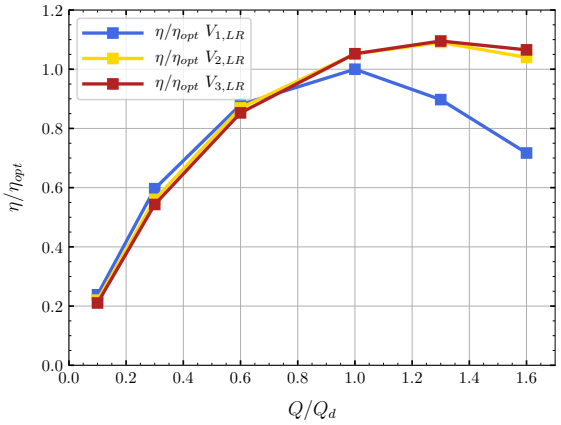

Figure 11. Efficiency calculated by CFD for Low-Reynolds number meshes.

At partload, the head is seen to flatten when increasing the volute throat area. The flattening of the head curve indicates more pump losses for a bigger volute. When using an impeller with a higher number of blades, higher blade outlet angle or higher outlet width, the head curve might be unstable. The study of the flow at partload is thus of interest.

The losses in each of the regions close to shut-off, at $Q/Q_d = 0.1$, are plotted in figure 12. It is seen that the losses are higher for the bigger volutes in all domains, except in the volute, where losses are the lowest.

To investigate these losses, the flow transfer among several planes is computed and visualized in figure 13. The figure describes the time-averaged normal velocity v_n at three planes. The velocity is scaled by the averaged inlet velocity v_{m1}. The three planes are located in the sidewall gap (hub side), at the outlet of the impeller and at the sidewall gap (shroud side). The velocity v_n is positive when the fluid flows into the volute, and negative when it flows out. For the sidewall gap (hub side), between 0 and 90 degrees, the exchange is at equilibrium, and v_n is close to zero. Between 90 and 250, there is a net flow from the sidewall gap into the volute. Between 250 and 360 degrees, the flow exits the volute at large speed. The last portion of the volute has a higher pressure, and drives the flow back to the suction. Additionally, with the impeller blade approaching the tongue, the flow is pushed into the gaps, leaving the volute. The averaged velocity v_n is negative, as the fluid flows back to the inlet of the impeller.

For the impeller, the process is cyclic, governed by blade passage. The large peak every 90 degrees shows that the flow exits the impeller on the pressure side. A backflow is clearly visible

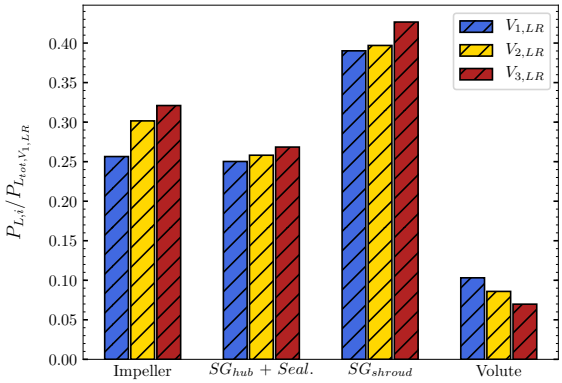

Figure 12. Relative losses per domain per case as per equation 4 at $Q/Q_d = 0.1$.

right after. Finally, there is no net flow exchange from the middle of the impeller to the suction side of the blade.

For the sidewall gap (shroud side), the averaged total flow is zero as it is a closed computational domain. From 0 to 180 degrees, the fluid flows from the gap into the volute. The flow is then close to 0 until about 250 degrees, and the fluid again exits the volute at high speed between 250 and 360 degrees.

The flow patterns are very similar for all volutes, but the exchange is stronger with bigger volute. The value of $|v_n|$ is higher for $V_{3,LR}$. In other words, the curve for $V_{3,LR}$ is always higher in the positive velocity region and always lower in the negative region. A bigger volute thus lead to a higher flow exchange between domains, and consequently higher losses, leading to a flatter head curve close to shut-off.

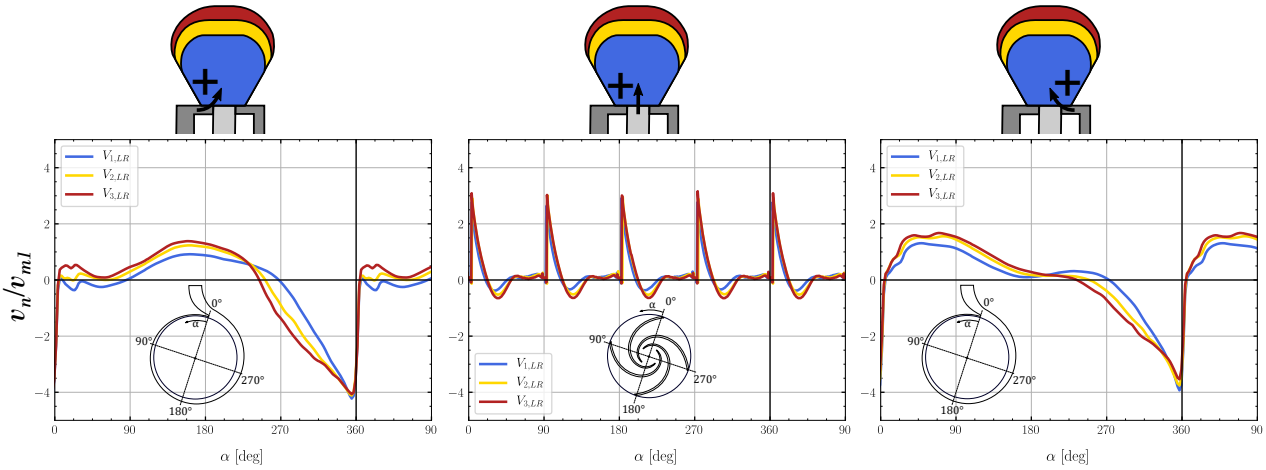

Figure 13. Illustrated circulation at different sections of the pump at $Q/Q_d = 0.1$.

5. Conclusion

The flow in a low specific speed pump of $n_q = 8.9$ has been computed by means of CFD. In the first part, it is seen that using wall-function approach leads to large differences in the predicted pump performances as compared to the low-Reynolds number approach. A fourty

percent difference is observed at $Q/Q_d = 1.6$ for the case V_1. The difference is due to a wrong prediction of losses downstream the volute tongue, where a zone or large turbulent kinetic energy is present. This mixing zone lowers in intensity as the volute throat area is increased, and so does the difference in prediction of performances between the two wall-modeling approaches.

In the second part, it is seen that increasing the volute throat area increases the performance of the pump at the best efficiency point and at overload. The reason for such an improvement is in the reduction of TKE downstream the tongue with a throat area enlargement. The source of overload losses suggests that the part downstream the tongue is a critical part. In the case of the first design V_1, a special care in the design of this region may reduce the observed losses to improve overload flow, while keeping the advantages of a steeper head curve at partload. Indeed, the head decreases at partload with larger volutes and the risk of instability rises. The flow close to the shut-off head ($Q/Q_d = 0.1$) is investigated. It reveals that a bigger volute leads to higher losses in all domains, except in the volute. The study of the flow exchange between domains (volute, impeller, sidewall gaps) shows that a bigger volute leads to a larger exchange of flow between domains, and so higher mixing losses and friction losses in the case of the sidewall gaps.

Acknowledgments

The research has been supported by project "Computer Simulations for Effective Low-Emission Energy" funded as project No. CZ.02.1.01/0.0/0.0/16 026/0008392 by Operational Programme Research, Development and Education, Priority axis 1: Strengthening capacity for high-quality research and by specific research project No. FSI-S-20-6235 of Brno University of Technology, Faculty of Mechanical Engineering.

References

[1] Wang Y, Wang W 2012 Applicability of eddy viscosity turbulence models in low specific speed centrifugal pump *IOP Conference Series: Earth and Environmental Science* **15** (6) pp 062013
[2] Limbach P, Kimoto M, Deimel C, Skoda R 2014 Numerical 3d simulation of the cavitating flow in a centrifugal pump with low specific speed and evaluation of the suction head *Proceedings of ASME Turbo Expo 2014* pp 1-9
[3] Juckelandt K, Wurm FH 2015 Applicability of wall-function approach in simulations of turbomachines *Proceedings of the ASME Turbo Expo 2015: Turbine Technical Conference and Exposition* **2B** GT2015-42014
[4] Worster RC 1963 The flow in volutes and its effect on centrifugal pump performance *ARCHIVE Proceedings of the Institution of Mechanical Engineers 1847-1982* **1-196** (177) pp 843-875
[5] Gulich JF 2014 Centrifugal Pumps Second Edition Springer-Verlag. ISBN: 978-3-642-12823-3
[6] Juckelandt K 2016 *Experimentelle und numerische Untersuchung der Strömung in Pumpen kleiner spezifischer Drehzahl unter Berücksichtigung des Rauheitseinflusses* Ph.D.thesis University of Rostock
[7] Khoeini D, Riasi A, Shahmoradi A 2017 Effects of Volute Throat Enlargement and Fluid Viscosity on the Performance of an Over Hung Centrifugal Pump *International Journal of Fluid Machinery and Systems* **10** pp 30-39
[8] Pochyly F, Stejskal J 2016 Rotational Flow in Centrifugal Pump Meridian Using Curvilinear Coordinates *J. Fluids Eng* **138** (8) 081101
[9] Stejskal J 2017 *Analysis of the velocity and pressure elds of the liquid using curvilinear coordinates* Ph.D.thesis Brno University of Technology
[10] Menter FR 1994 Two-Equation Eddy-Viscosity Turbulence Models for Engineering Applications *AIAA* **32** pp 1598-1605